0.1 High-Energy Astrophysics

0.1.1 Introduction

Theoretical Astrophysics and experimental High-Energy Astrophysics are complementary fields of investigation at the MPI für Kernphysik. Some of the more phenomenological theoretical work is reported here in juxtaposition with the joint project on Very High Energy γ-ray Astronomy with imaging atmospheric Cherenkov telescopes of the Astrophysics and the Particle Physics divisions of the institute.

In this section of the report, four different research areas are adressed:

- The CRT project study.
- The installation of the stereoscopic HEGRA Cherenkov telescope array and its results regarding the detection of cosmic TeV gamma-ray sources.
- The modelling of cosmic gamma-ray sources.
- The activity concerning a future telescope system.

0.1.2 The CRT project

will be submitted by K.Bernloehr

0.1.3 Imaging Atmospheric Cherenkov Telescopes at La Palma

F. Aharonian, A. Akhperjanian[a], A. Daum, A. Fraß, M. Hemberger, G. Hermann, M. Heß, A. Heusler, W. Hofmann, R. Kankanian[a], C. Köhler, A. Konopelko[b], T. Kutter, H. Lampeitl, M. Panter, G. Pühlhofer, M. Ulrich, H.J. Völk, C.A. Wiedner, H. Wirth.

[a]Yerevan Physics Institute, Armenia
[b]Altai State University, Barnaul, Russia

Imaging Atmospheric Cherenkov Telescopes are today considered to be the most effective experimental technique for the investigation of cosmic γ-rays in the energy range of TeV. A new approach is realized by the HEGRA collaboration by building a system of 5 IACTs. The benefit of a system of telescopes is based on the stereoscopic view of an air shower. The stereoscopic view provides sufficient information for the full reconstruction of the direction and core position of the shower, leading to an improved energy determination and the possibility to detect extended γ-ray sources. In this section we describe the installation and operation of the new telescope system as well as analysis results of the two HEGRA prototype telescopes and the IACT system.

Operation and observations overview

During the first seven months of 1996 three telescopes were operating. The prototype CT1 [1] with a 127 pixel camera, the prototype CT2 [2] with a 61 pixel camera and CT3 [3] with a 271 pixel camera. All three telescopes were running in a stand alone data taking mode, but the start of data runs as well as the targets of observation were synchronized. Thus offline event synchronization was made possible by a commonly used event time tag.

In order to study the performance of the new system telescope CT3, observations began with the Crab Nebula, the "standard candle" in TeV gamma astronomy.

More data was taken observing WComae, MRK421 and GRS1915 with CT1+2+3 in synchronized mode. From March onwards the prototype telescope CT1 was part time operating separately from the other telescopes for observing additional targets of interest and performing technical investigations.

During 1996 three new system telescopes similar to CT3 were coming into operation. When CT4 started to operate in August, the data taking modus was changed to a system trigger scheme, allowing for better background rejection and lower trigger threshold. The two system telescopes CT3+4 started data taking in a combined system data acquisition, including online event building. Investigations of potential γ-ray sources started immediately by observing the supernova remnant G78.2+2.1 . These observations were continued by the three telescope system CT3+4+5 from September onwards. Some data was taken from the standard candle Crab Nebula to investigate the performance and sensitivity of the 3(4) telescope system. In december the system was enlarged by taking CT6 into operation.

In total 11 astrophysical objects have been observed by the six HEGRA telescopes in 1996. The observation times for those objects which were studied with $\geq$ 2 telescopes are shown in table 0.1. Note that most of the objects where observed in the so called On-Off mode which im-

Telescope	1	2	3	4	5	6
Crab	102	94	98	55	55	10
MRK421	82	149	143	-	2	2
GRS1915	-	176	164	35	-	-
G78.2+2.1	-	189	159	162	86	-
MRK501	274	10	1	-	-	-
1ES2344	-	36	33	33	33	3
WComae	20	17	20	-	-	-
IC443	-	-	2	1	2	2
Σ	478	671	620	285	178	17

Tab. 0.1: Main targets of observation of the HEGRA telescopes in 1996, i.e. targets which have been observed by several telescopes. The quoted numbers are hours of observation time.

plies that half of the quoted observation time was used for background determination. The prototype telescope CT1 was used to observe additional targets which are not contained in this table. The available observation time was reduced by technical problems ($\approx 4\%$), necessary calibration runs ($\approx 4\%$) and an unusually large fraction of bad weather conditions ($\approx 37\%$, most of it during winter time). The new system telescopes CT3+4+5+6 also required some additional time for hard- and software testing necessary for running in the system.

Results of CT1 and CT2 data analysis

During the last several years CT1 and CT2 have been used to search for TeV γ-rays from a variety of astronomical objects. First, a positive signal of γ emission was seen from the Crab Nebula in 1992 by CT1 in its first version [1]. Based on the data set of observations in winter 1994/1995 we have detected TeV γ-rays from the Crab Nebula with a significance of $\sim 10\sigma$ using CT2 [4]. Observations of Markarian 421 in 1995 resulted in the independent detection of statistically significant positive signals by CT1 and CT2 [6], thus confirming the discovery by the Whipple collaboration of TeV emission from this BL Lac object [7].

While the 5-IACT system is nearing the final stage of its commission, in 1996 we continued to use the available telescopes in different configurations not only for methodological investigations, but also for further observations of potential γ sources. We allocated an essential part of observation time for the BL Lac Mrk 501 and the galactic Microquasar GRS 1915+105. In the following we briefly discuss the results obtained from data of those two objects.

Results of Mrk 501 data analysis. This source is very similar to Mrk 421, and belongs to the same sub-population of AGNs called BL Lac objects - highly variable AGNs without strong emission lines, but showing a strong nonthermal component of radiation from radio to X-ray wavelengths. Recent EGRET observations showed that these objects are effective γ-ray emitters at energies $\geq 100\,\mathrm{MeV}$ [8]. Although Mrk 501 is not in the list of γ-ray emitting BL Lac's detected by EGRET, this source has been reported by the Whipple group to emit γ-rays above 300 GeV at an average flux level of approximately 10% Crab [10]. The low flux of VHE γ-radiation from this source makes its detection rather difficult for our prototype CT1 and CT2 telescopes. However, in the beginning of this year Mrk 501 started to show a flaring activity in VHE γ-rays (Weekes, private communication). This motivated us to allocate the CT1 for long-term observations of Mrk 501. In order to obtain maximum exposure time the source was observed in tracking mode. Almost 150 hours of good quality data were obtained at zenith angles $\leq 25°$ during the period March-August 1996. The OFF-source observations required for background determination were made when Mrk 501 was not observable.

object	Mrk 501	Crab
ON-source obs. time [h]	146.8	22.9
ON events after all cuts	1325	423
expected background	974	237
number of excess events	351	186
excess rate [h^{-1}]	2.4	8.1
stat. significance(Li& Ma [9])	5.2	7.6

Tab. 0.2: Summary of Mrk 501 and Crab observations with CT1.

The α-distribution[1] for Mrk 501 shown in Fig. 0.1 indicates an excess of 351 events over expected 974±57 background events (see Table 0.2) which can be interpreted as detection of γ-rays

[1]see [14] for the definition of the α parameter

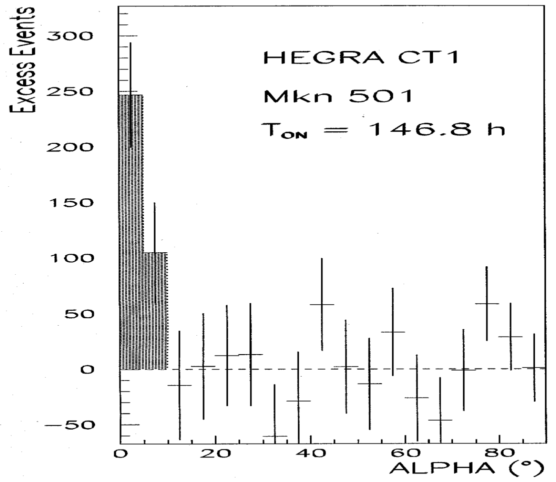

Fig. 0.1: The α-distribution of the excess events for Mrk 501.

with a rate $R_\gamma \simeq 2.4\,\mathrm{h}^{-1}$ and statistical significance of 5.2σ [11]. Using the same procedure we find an excess rate of γ-like events from the direction of the Crab Nebula of $R_\gamma \simeq 8.1\,\mathrm{h}^{-1}$. This implies that during the observation period the flux from Mrk 501 was ≈ 3 times lower than the Crab flux, i.e. approximately $2.5\times10^{-12}\,\mathrm{ph/cm^2s}$ ($E_\gamma \geq 1.5$ TeV). For comparison, the Whipple observations of Mrk 501 in 1995 showed a lower flux relative to the Crab ($\approx$ 10%) at energies $\geq 300\,\mathrm{GeV}$. This can be explained by different energy spectra of the Crab and Mrk 501 and/or by a strong variability of Mrk 501 which can be significant on timescales of 1 day [10].

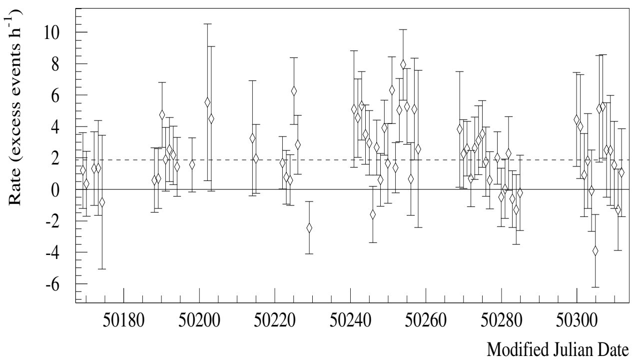

Fig. 0.2: Daily excess γ-ray event rates from Mrk 501.

The daily excess γ-ray event rates of our data are shown in Fig. 0.2. Unfortunately the low counting statistics does not allow a definite conclusion concerning the variability of the source. The analysis of the distribution of the total light content in the camera does not show a significant deviation of the spectral shape of Mrk 501 from the Crab spectrum, but the uncertainty in the estimated power-law index , -2.6 ± 0.5, is too large to allow a strong statement about the spectral characteristics of the source.

Results of GRS 1915+105 data analysis. The recent discovery of the galactic superluminal source GRS 1915+105 [12], the scaled-down analog of the AGN jets which are recognized as high energy γ-ray emitters, motivated the HEGRA collaboration to put this "microquasar" in the "Targets of Opportunity" list.

The first observations of the source in spring 1995 with the telescopes CT1 (13 h) and CT2 (25 h) in ON/OFF mode showed weak evidence for a signal with statistical significance 2.8σ and 2.6σ, respectively. However, the observations with the same telescopes after Aug 15th with doubled exposure time did not reveal any indication of a positive signal. Since this might be a result of a highly sporadic behavior of GRS 1915+105, we decided to continue observations in 1996.

In 1996 GRS 1915+105 has been observed during the period May-July 1996 by CT2 and CT3.

CT2 with an energy threshold $\approx 1\,\mathrm{TeV}$ had been successfully used earlier for observations of the Crab Nebula [4] and Mrk 421 [6]. Based on the observations of the Crab Nebula the sensitivity of CT2 is estimated as $\approx 1.25\sigma/\sqrt{\mathrm{h}}$ detection rate of a signal from a point source at the flux level $J_\gamma(\geq 1\,\mathrm{TeV}) \approx 10^{-11}\,\mathrm{ph/cm^2s}$. This parameter has not been changed noticeably during the last 2 years which demonstrates the high stability of operation of the CT2 telescope.

Since GRS 1915+105 is a highly variable object, we observed the source in tracking mode. In addition, each month certain ON/OFF pairs were taken in order to monitor the shape of the background "α-distribution". The statistics of observations at zenith angles $\theta \leq 30°$ and the results are summarized in Table 0.3. The α-distribution of ON-OFF source events shown in Fig. 0.3 indicats a possible signal with a statistical significance of 4.7σ. The average rate of excess events is $\approx 4\,\mathrm{h}^{-1}$, which corresponds to $\approx 25\%$ of the γ-ray detection rate from the Crab

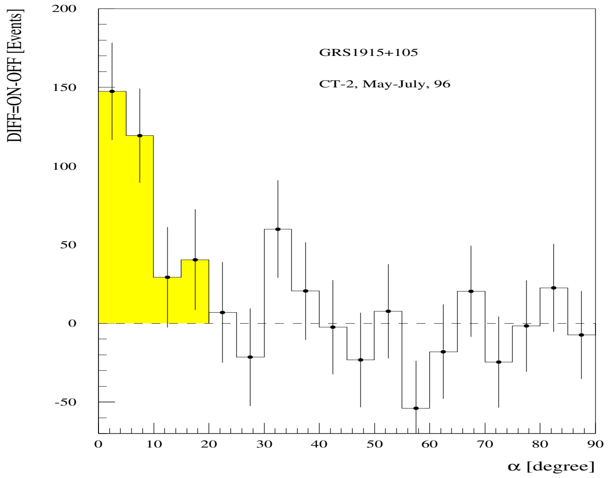

Fig. 0.3: The α-distribution of the excess events for GRS 1915+105.

	May	June	July	Total
ON-source obs. time [h]	9.89	37.12	23.83	70.84
ON events after all cuts	427	1527	944	2898
expected background	365	1373	875	2612
number of excess events	62	154	69	285
excess rate [h^{-1}]	6.2	4.2	2.9	4.02
stat. significance (Li& Ma [9])	2.68	3.46	1.95	4.66

Tab. 0.3: Summary of GRS 1915+105 observations with CT2.

Nebula using CT2. Note that most of the excess events were obtained in the June period of observation which can be explained by $\approx$ 50% of statistics contained in this period. At the same time one cannot exclude an intrinsic variability of the signal itself. For example, the statistical significance of the signal in June 19 data alone is of about 3σ, with a rate exceeding the average rate by a factor of 3. This can be seen in Fig. 0.4 where we present the daily rates of the excess events. Another feature of the time profile of the rate is its rather interesting coincidence with 3 prominent few-day-duration flares of GRS 1915+105 detected in radio and X-ray energy regime. This possible correlation may serve as an additional argument that strengthens the belief that the TeV γ-ray detection from this source is a real effect rather than a result of statistical fluctuation of the background. If so, assuming that the radiation originates in the jet of GRS 1915+105 approaching us, the intrinsic average TeV luminosity of the source is estimated to be 10^{36} erg/s.

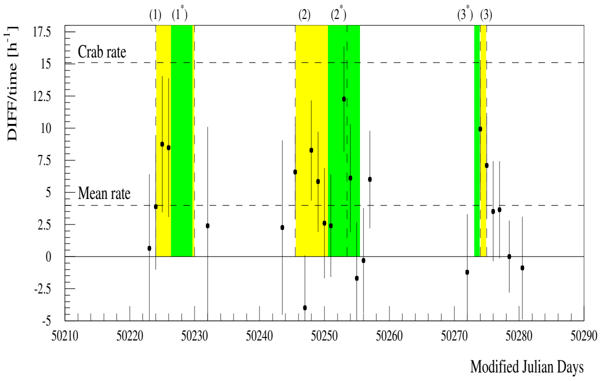

Fig. 0.4: Daily rates of the excess events from GRS 1915+105. For comparison, the periods of large outbursts in radio and X-rays also are shown. The light hatched zones (1,2,3) with borders indicated by dashed vertical lines corresponds to the periods of X-ray flares reported by Greiner J. et al., (Ap.J. Letters (in press); IAU Circ.6435), and the dark hatched zones $(1^*, 2^*, 3^*)$ correspond to the radio flares detected by the Ryle and Nancay telescopes (IAU Circ. 6411; 6432). A strong hard X-ray outburst in May 24-27 (MJD 50228-50231) has been reported also by the BATSE team (IAU Circ.6411). Note that at the time intervals without γ-ray data points correspond to the moonlight periods when the source could not be monitored.

However, we would like to emphasize that before going too far in the astrophysical interpretation of this statistically marginal signal, we obviously need independent confirmation of this result by other instruments and groups. As mentioned before, the source was observed simultaneously also by the CT3 telescope. At the Perpignan Symposium [13], a positive signal was also reported from this telescope. Further analysis of these data however has revealed evidence for hardware problems during this observation period in some of the CT3 camera pixels, resulting in large spurious signals, which may fake γ-ray topologies. Work is in progress to correct these problems with adaquate offline software and to reprocess the data. At this point, no statement concerning GRS 1915+105 detection in CT3 data can be made. Thus the final interpretation of the CT2 data analysis has to be postponed.

Operation and data analysis of CT3

CT3 was the first system telescope with the final version of the camera, readout electronics and data acquisition system. When it came into operation in Oct. 1995, data was taken from the "standard candle" Crab Nebula in order to probe the performance and sensitivity of this new instrument. The encouraging results of the data analysis of the Crab season 1995/1996 are presented below. Based on the confidence arising from the Crab data analysis, it was decided to immediatly use the new telescope CT3 to study other objects of physical interest. The analysis of these data sets is still underway.

By comparing observation times listed in table 0.1 of CT3 and CT2, which is in operation since Dec. 1993, one can conclude that the uptime of the new instrument was nearly equal to the well understood older instrument (the observation schedules of CT2,3 were identical, so differences in observation time arise from technical problems and necessary testing for system commissioning).

Results of Crab Nebula data analysis. In order to investigate the benefit of the new high resolution camera of CT3 and to explore the threedimensional reconstruction of air showers, the Crab Nebula dataset 1995/1996 was analyzed by applying two different methods. First, some standard image cuts were applied, which are not sensitive to the shower direction but enrich primary gammas. In the second step the following methods to probe for a excess from the direction of the Crab Nebula were employed:

1. By using the 1-dimensional orientation parameter α, a sensitivity of $2.3\sigma/\sqrt{\mathrm{h}}$ statistical significance could be achieved [14].

2. By using the full information available in the high resolution camera, one can fit image distributions obtained from Monte Carlo simulations to the measured images, resulting in a 3-dimensional reconstruction of the shower direction and thus the distribution of excess events in the two angular dimensions of the field of view [15].

The result of the first analysis (see Fig 0.5) shows the improved sensitivity of CT3 compared to the prototype telescope CT2 (see above).

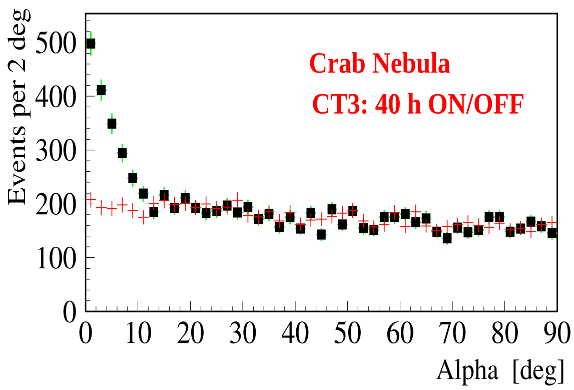

Fig. 0.5: The α-distribution of the ON and OFF (crosses) data sample for Crab Nebula CT3.

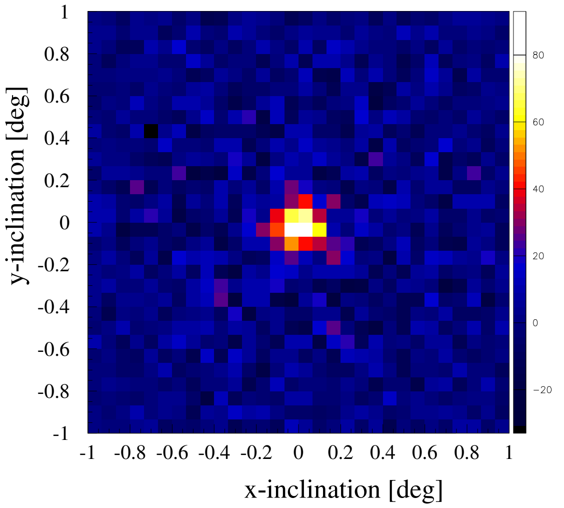

Fig. 0.6: The 2-dimensional distribution of excess events from the Crab Nebula region. A 2°x2° field of view is shown. The measured excess peak coincides with the Crab Nebula coordinates known from X-ray measurements.

The second method provided for the first time a two dimensional view of a TeV γ-ray source, see Fig 0.6. The sensitivity is comparable to the first method, but requires extensive computer usage. The obtained shape of the excess event distribution can be interpreted as a pointlike γ-ray source convoluted with an experimental angular resolution of 0.15° in the direction of the long symmetry axis of the elliptical image and 0.08° in the direction of the short axis.

The total amount of excess events was $\approx 10^3$ events, leading to a positiv Crab signal of $\approx 14\sigma$ statistical significance.

HEGRA Stereoscopic System of IACTs

The heart of the HEGRA IACT system are the five 8.5 m^2 telescopes CT2 through CT6, which will be equipped with 271-pixel cameras of 0.25° pixel size and the modern flash-ADC readout. Stereoscopic observation of air showers allows a full reconstruction of the shower axis and the shower impact point, thereby generating genuine source images like in normal optical telescopes. The knowledge of the core location allows an improved energy determination and the detection of spectral features such as cutoffs, and optimally matched cuts to isolate γ-induced air showers. In last year's annual report, the initial operation of the first of the system telescopes, CT3, was discussed. In 1996, all but one of the remaining telescopes were finished, and data was collected with up to four telescopes in coincidence.

Installation of the system telescopes. During the year 1996, the telescopes CT4, CT5, and CT6 were brought into operation. The installation of the mounts and mirror dishes was to a large extent carried out by MPI Munich, the following installation of the cameras, of the electronics, the adjustment of the mounts and mirrors, and the software installation and tests by MPI Heidelberg. The whole procedure, from the arrival of a camera at La Palma up to the point where a telescope went into routine shift operation lasted about 4 to 5 weeks, equivalent to about 20 man-weeks of physicists and technicians on site at La Palma. Especially the EN-workshop and the electronics workshop members of MPIK were involved in the work on the island. Fig. 0.7 summarizes the installation schedule, which also included modifications of the readout electronics. The initial telescope with a 271-pixel high-resolution camera, CT3, used a new flash-ADC system, developed by the MPIK electronics workshop [2], operated at 100 MHz sampling frequency.

[2]developed in cooperation with A. Walenta, Univ. Siegen

Experience with these modules resulted in a revision of the design, which delayed the production of the FADC modules for the remaining cameras. As an interim solution, an existing 40 MHz system was adapted, and used for CT4 and CT5. Late in 1996, the revised FADC modules became available, now capable of running at 120 MHz, and were installed in CT3, CT5, and CT6. CT4 will be upgraded in Feb. 1997. To complete the CT system, the telescope CT2 - the initial prototype of the system telescopes, so far equipped with a 61-pixel camera - has to be upgraded with a new camera and readout. The camera is ready; the readout modules will be available in spring 1997. Before installation of the camera, CT2 needs a modification of the mechanics of the mirror dish, to match the optical performance and stability of CT3 to CT6.

In response to a number of broken mirrors - so far, 20 out of the 150 mirrors installed showed cracks - a new mirror support was designed to reduce tensions on the mirrors, by connecting the support rods to a triangle behind the mirror rather than to the mirror directly; CT6 is equipped with these modified supports. Experience will show if this measure cures the problem.

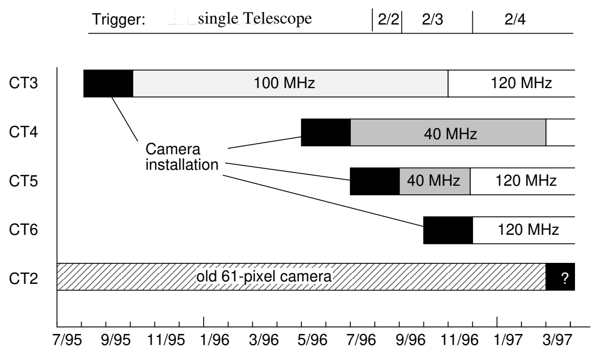

Fig. 0.7: Schedule of the installation of the cameras of the HEGRA CT system. In August 1996, the trigger was changed from a single-telescope trigger to a multi-telescope coincidence.

Geometry calibration. The stereoscopic reconstruction of air showers is very sensitive to deviations from the exact pointing of the telescopes. A first step after the installation is the alignment of the vertical axis and the survey of a telescope by means of a theodolite. The final calibration of telescope pointing is then based on so-called "point runs". In these runs, the image of a star is scanned in fine lines across one or more pixels, and the DC currents of the camera PMT's are measured. For a given position of the image, the current is proportional to the point spread function of the mirror, integrated over the pixel area. From such scans, both the location of the image - and hence pointing deviations - as well as the width of the point spread function can be determined. During 1995, this technique as well as the understanding of pointing deviations has improved considerable [16], to match the increased requirements which became obvious when the reconstruction of system data began. Figs. 0.8 (a),(b) illustrate the differences between the nominal positions of stars, and their observed images, as a function of altitude and azimuth. In some areas, deviations exceed 0.2°. These data are then fitted with a model of pointing deviations including atmospheric refraction and, as free parameters,

- the bending of the camera masts (assumed to be proportional the $\cos(altitude)$),
- an offset of the camera from the optical axis of the telescope,
- a deviation of the azimuth axis from vertical alignment,
- an offset in the shaft encoder values measuring azimuth and altitude,
- a modulation of the azimuth shaft encoder, e.g. due to eccentricity of the axes or gears.

This model provides a consistent description of the data; after a corresponding correction, all star images appear at their nominal positions, with a rms deviation of less than 0.005° (see Fig. 0.8 (c)), sufficiently precise for the most ambitious reconstruction techniques.

Calibration of telescope sensitivity. A crucial issue for the determination of γ-ray fluxes from galactic and extragalactic sources is the energy calibration of the telescopes, i.e. the relation between the shower energy and the amplitude of an image, ultimately measured in units of ADC counts. This calibration involves the Cherenkov emission by air showers, the propagation of Cherenkov light in the atmosphere,

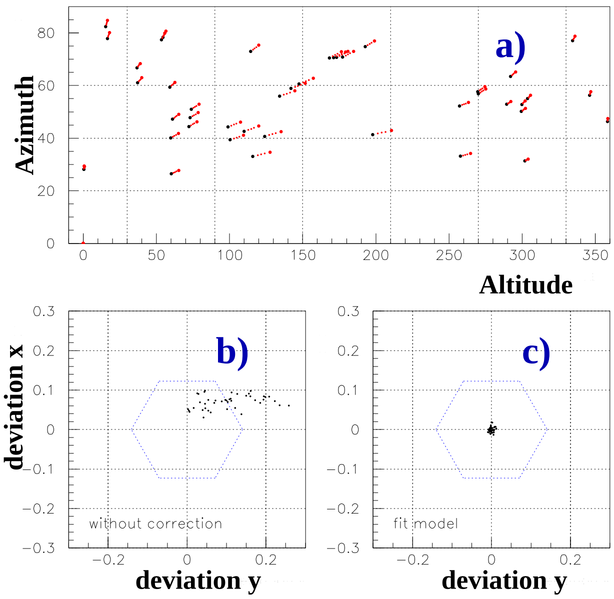

Fig. 0.8: Top: pointing deviations of one of the HEGRA telescopes as a function of azimuth and altitude, determined using images of bright stars. The (enlarged) deviations are indicated as vectors. Bottom left: measured deviations from the nominal pointing for an ensemble of stars. For comparison, the outline of a 0.25° camera pixel is superimposed. Bottom right: deviations after correction using the model discussed in the text.

the effective mirror area of the telescope, the reflectivity of the mirrors and light collectors, the quantum efficiency of the PMTs, the gain of the PMTs, and the various electronics conversion factors. A number of techniques are used for this energy calibration, generally combining estimates (or Monte-Carlo simulations) for some of the factors, with measurements for others. The analysis of CT2 Crab data e.g. tried to derive an overall calibration factor from the comparison of measured and observed cosmic-ray detection rates; other approaches use muon ring images for calibration. All these techniques require to some degree assumptions and extrapolations, and results are frequently not fully consistent.

During 1996, a new approach was tested which allows to measure the overall calibration factor relating the flux of photons incident on the telescope to the ADC response. A pulsed, frequency-selective light source is placed about

60 m from a telescope, such that the mirror is uniformly illuminated. The light source consists of a Nitrogen laser, an attenuator ($\approx 10^{-3}$), a scintillator, and band filters. The scintillator shifts the laser light to wavelengths between 350 nm and 500 nm, with basically isotropic emission. At a distance of 60 m, the IACT camera is not in focus; the source illuminates, via reflection in the mirror, the camera more or less uniformly with the exception of the outer two rings of pixels, which remain dark. The intensity of the source is adjusted to match the dynamic range of the camera, generating about 100 to 200 photoelectrons per pixel, or some 10^4 photoelectrons in total. To determine the overall response of the telescope as the ratio of the sum of ADC counts to the incident flux, the flux of the source has to be determined. At the low light level used to illuminate the camera, this is virtually impossible. Therefore, the attenuator in the laser beam is removed, and a calibrated photodiode mounted on the telescope is read out via a low-noise preamplifier. With this arrangement, light pulses of 10^4 photons/cm^2 can be detected, and the mean flux of photons determined with sufficient precision by averaging over many pulses. As a final step, the attenuator is calibrated with the laser beam and a photometer with large dynamic range.

Two sets of measurements were carried out in La Palma, together with systematic studies in the laboratory, related to the response and effective area of the reference diode and the precide determination of attenuation factors [17]. The measurements demonstrated the feasibility of the technique and provided calibration factors at two wavelengths, 430 nm and 470 nm. The uncertainty of the calibration constants derived by this technique is less than 10%; they are in good agreement with previously assumed conversion factors.

Multi-telescope trigger. One of the benefits of a system of IACTs is that by requiring a coincidence between two or more telescopes, the rates of fake triggers due to night-sky background or local muons can be drastically reduced. As a result, the telescopes can be operated with reduced trigger thresholds and energy thresholds.

The multi-telescope coincidence trigger uses trigger signals generated by the individual telescopes (typically a two-pixel concidence), which are routed to a central trigger station. To implement the telescope coincidence trigger, a custom VME unit was developped, which includes computer-controled delays for the trigger signal from each telescope, and a majority unit allowing to require at least N out of M telescopes. The delays are required to compensate differences in the timing, due to the fact that an inclined Cherenkov light front does not reach all telescopes at the same time. The delay values are continuously updated as the observed object moves across the sky. Once a telescope coincidence trigger is generated, a trigger signal and an event number is generated and sent back to the individual telescopes. The trigger distribution uses the so called "event grader" master and slave VME units originally developped for the CRT project. This central trigger arrives at the telescopes with a delay of about 1 μs after the Cherenkov light; at this point, the FADC converters are stopped (which provide 33 μs of signal history), and the relevant range of time slices is read out, buffered, and sent to a central event builder, where data from all telescopes are assembled into a single data stream. Due to the recording of signals with FADCs, all telescopes are read out, even those which did not themselves generate a trigger signal, but which still may provide useful images.

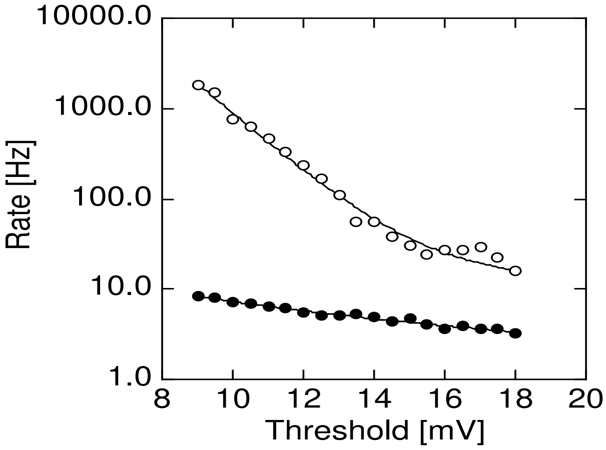

Fig. 0.9: Rate of single telescope triggers (open points) and two-telescope coincidence triggers (filled points), as a function of the trigger thresholds applied for the camera pixels. To trigger a telescope, two pixels had to exceed this threshold; 1 photoelectron is roughly equivalent to 1.2 mV.

Before the system was routinely operated in a multi-telescope coincidence mode, various systematic studies were carried out to ensure the proper functioning and understanding of the coincidence trigger. Setting the computer-controled delays to compensate for the expected delays between telescope signals, signals from different telescopes were found to coincide within 10 ns rms, with systematic shifts around 10 ns. The hardware coincidence window of 70 ns safely includes all genuine coincidences. The single-telescope and two-telescope rates are illustrated in Fig. 0.9.

The single-telescope rate shows a very steep dependence on the trigger threshold. At thresholds below 15 mV, triggers are almost entirely caused by random combinations of pixels triggered by night-sky background; for higher thresholds, genuine air showers begin to take over, and the dependence flattens. The two-telescope coincidence shows over the entire range a dependence consistent with the power-law spectrum of air showers; the fraction of random coincidences is small even at the lowest thresholds. The system is therefore typically operated at pixel thresholds of 10 mV, equivalent to an energy threshold of 0.5 TeV. Even lower thresholds are in principle possible, but then the number of photoelectrons contained in a typical image is too small for a meaningful image analysis.

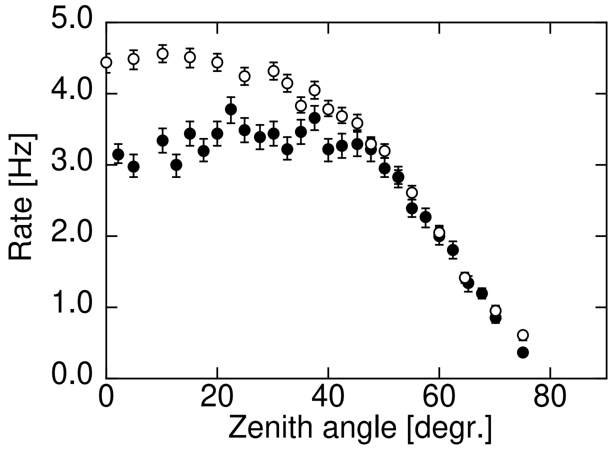

Fig. 0.10: Rate of single telescope triggers (open points) and two-telescope coincidence triggers (filled points), as a function of the angle from the zenith. Trigger thresholds were set differently for the single-telescope and the two-telescope mode, such that in each case the fraction of random triggers was small, and only genuine air showers trigger.

Fig. 0.10 illustrates how the single-telescope rate and the two-telescope coincidence rate depend on the zenith angle, at which the telescope is pointing. Both rates are relatively flat out to 45° from the zenith and drop steeply at lower altitudes. The ratio between two-telescope triggers and single-telescope rates increases with zenith angle; the reason is that with larger zenith angles the distance between the telescopes and the shower maximum increases, as well as the diameter of the light pool. It is then more likely to have both telescopes in the light pool. At zenith angles beyond 45°, the intensity of light in the Cherenkov pool decreases and the energy threshold increases rapidly.

For all multi-telescope trigger data discussed so far, the telecopes were pointing parallel to each other. Fig. 0.11 shows the variation of the rate with the angle between the optical axis of two telescopes; positive angles mean that the telescopes are tilted inward towards each other, along the line connecting the telescopes.

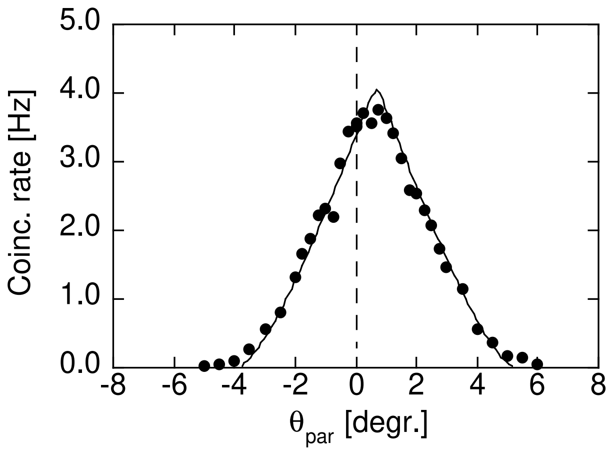

Fig. 0.11: Two-telescope coincidence rate as a function of the difference in pointing of the two telescopes; the telescopes are tilted against each other along the line joining the telescopes. The solid line indicates the overlap of the fields of view at the height of the shower maximum.

The interpretation of the data is possible in a simple geometrical picture: a telescope triggers when the shower maximum (in about 6 km height) is in its field of view (which has a diameter of about 4.3°). The peak coincidence rate is obtained when both telescopes point at the same location at about 6 km height, i.e. are slightly inclined towards each other. In general, the trigger rate is basically proportional to the overlap of their respective fields of view (solid line in Fig. 0.11). For a tilt perpendicular to the interconnection line of the telescopes, the rate curve is of course symmetric around zero, but otherwise similar in shape.

These and many other studies [18] confirmed that the multi-telescope trigger behaves as expected. In consequence, the trigger for the system telescopes was changed to a two-telescopes coincidence in August 1996, initially with two out of two telescopes (CT3,4), later with two out of three (CT3,4,5) and four (CT3,4,5,6) telescopes (see Fig. 0.7).

Pulse shape analysis. The new HEGRA cameras are read out with 120 MHz FLASH-ADC systems, which record the complete pulse shape of the signal from each pixel. Compared to a conventional read out, this system has a number of advantages:

- Since data are stored in digital form, a decision to read the event can come several μs after the event.
- The timing of signals can be determined with a precision of 1 ns or better.
- Background and noise signals can be identified on the basis of their shape and timing.
- The pulse shape may help in the γ-hadron separation.

The analysis of FADC data to extract and summarize the relevant information is non-trivial, and significant effort was dedicated to this task. The following procedure emerged: pedestal values are continuously tracked and updated based on FADC samples before and after the shower signals. For pulses which do not saturate the FADC dynamic range, the signal is digitally deconvoluted; the deconvolution reverses the effect of the signal shapers in front of the FADC, which suppress frequency components above the Nyquist frequency of the FADC. After the deconvolution, the signal should approximate the initial δ-function pulse describing the generation of a photoelectron, and should be concentrated in subsequent time slices. Fig. 0.12 illustrates the signal shape before and after deconvolution.

The main reason for the deconvolution is that the net signal integration time and hence the influence of sky noise is reduced [19]. A signal timing is defined as the c.o.g. of the deconvoluted pulse, after correcting for channel-dependent timing shifts determined from laser calibration data. The deconvolution assumes a linear response and cannot be applied to signals saturating the 8-bit dynamic range of the FADC. In such cases, the area under the raw signal is determined, and is converted into a signal amplitude on the basis of a lookup-table; for the pulse with a time profile of $t\exp(-t/\tau)$ after the shaper, the area of overflow pulses is roughly proportional to the logarithm of the original pulse amplitude. In this way, the dynamic range of the system can be increased by a factor $\approx$2, up to about 500 photoelectons per pixel (the linear range ends at about 245 photoelectrons). For even larger light pulses, nonlinearities in the PMT and preamp become important. An average event timing is determined on the basis of those pixels with large (> 8 photoelectrons) signals. Two amplitudes are made available to the user: the amplitude calculated from the two maximum bins of the deconvoluted signal (or the corrected amplitude sum for overflow pulses), and the signal intensity in the two FADC samples around the average event time. For small signals influenced by noise, the second method represents basically a matched filter, optimally extracting a signal in the presence of noise.

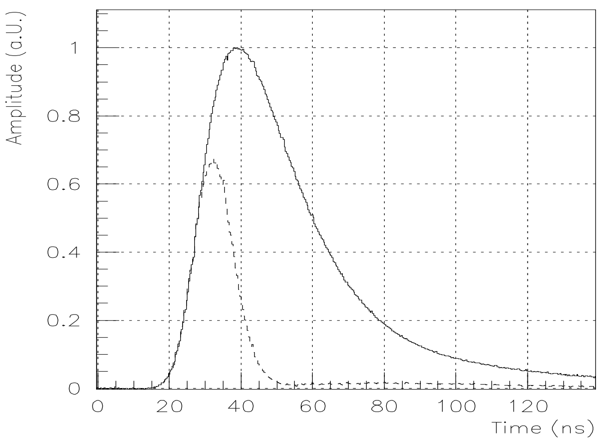

Fig. 0.12: Averaged PMT signal before and after the digital deconvolution of the FADC data.

An interesting result of these studies was that while for most events all pixels exhibit signals at the same time, there are some events with a wide dispersion of signal arrival times between pixels (Fig. 0.13).

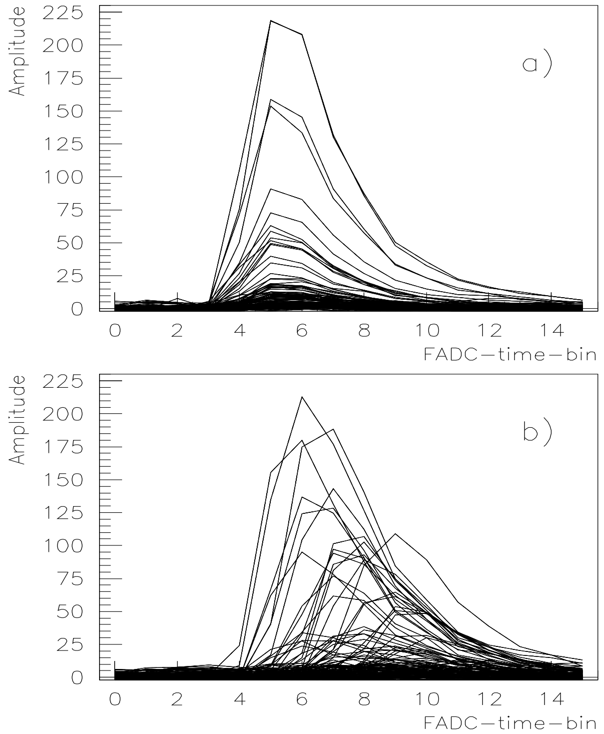

Fig. 0.13: FADC signals for a typical event (top), with all signals arriving at the same time, and for an event with a large variance in arrival times (bottom).

On the basis of the stereoscopic reconstruction of the events, these anomalous events could be identified as cases where a high-energy shower has a rather distant impact point, and forms a large angle (of order 3° to 5°) with the telescope axis. While the telescope is outside the genuine Cherenkov light pool, such events can still trigger, provided the shower energy and hence the light yield is very high. For such oblique showers, there is a difference of some 10 ns between the light arriving from the head and the tail of the shower, and hence a gradient of pixel timing across the image.

Obviously, the timing information can be exploited to provide important clues for the reconstruction of showers; the work discussed here represents only the initial steps.

First analysis of system data. While a number of sources were observed in stereoscopic mode with 2, 3, and 4 telescopes, data analysis concentrated on the observations of the Crab nebula, which is used as a “standard candle”, and which serves to develop and optimize the reconstruction procedure. Partly due to bad weather, the ON data samples available so far are limited to 8 h of 3-telescope observations, and about 2 h of 4-telescope observations. Data analysis is hampered by the fact that some calibration data - in particular concerning CT6 - are still missing.

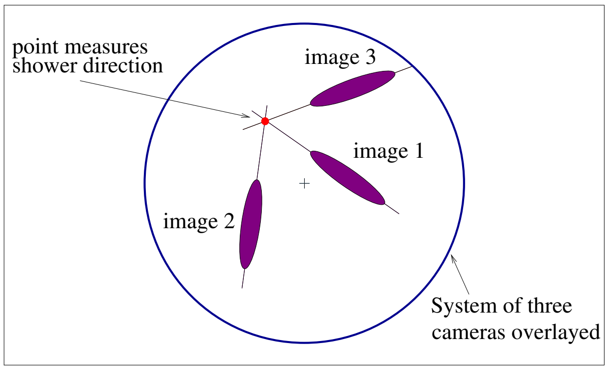

Fig. 0.14: Reconstruction of the shower direction. The image of the apparent source of an air shower has to lie on the symmetry axis of the Cherenkov image. The direction of the shower is hence given by the point where the axes of images of the different telescopes intersect.

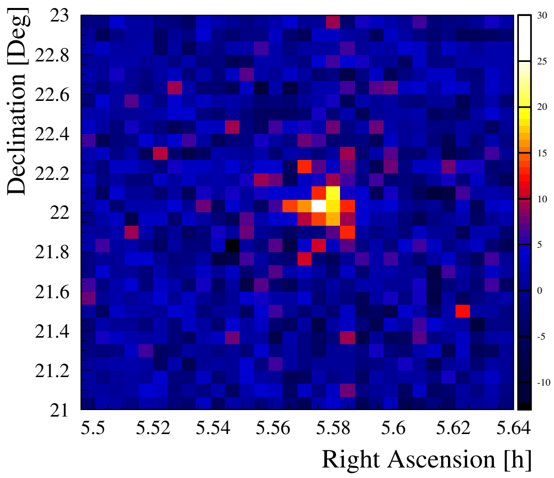

Fig. 0.15: Distribution of reconstructed air showers from 8 h Crab data ON-OFF CT3+4+5, after ”loose cuts” to select γ-ray candidates. The excess in the center coincides with the location of the Crab Nebula.

The system data were analyzed in two ways, once in the conventional fashion - shape cuts to select γ candidates and cuts on the orientation of the events, in particular the *distance* between image and camera centers, and the angle α between the image axis and the direction to the camera center, i.e. the image of the source. Showers pointing towards the presumed source should perferentially have *distance* values between about 0.5° and 1.1°, and point to the camera center. The second analysis is based on the geometrical reconstruction of the shower axis, see Fig. 0.14 and the discussion in last year's annual report.

In either mode of analysis, clear Crab signals were visible both in the 3-telescope and the 4-telescope data sets. Fig. 0.15 shows the distribution of shower directions obtained from the geometrical reconstruction, with a clear excess at the location of Crab Nebula.

Despite the short observation time - only 2 h for the sample shown, the excess is highly significant (Fig. 0.16). The peak has a gaussian width of 0.1°, consistent with the expected angular resolution for the IACT system.

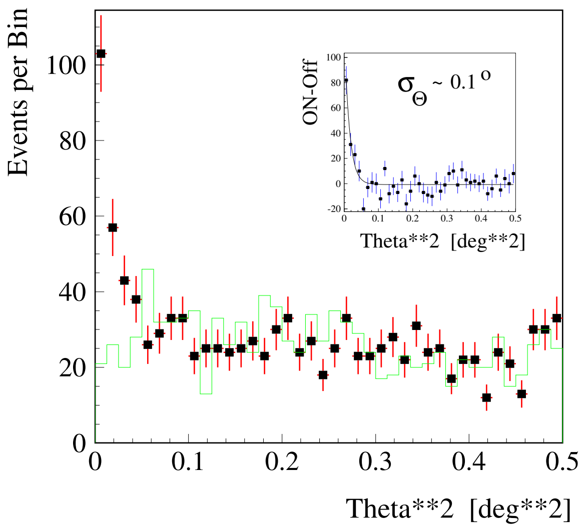

Fig. 0.16: Distribution of geometrically reconstructed shower axes relative to the direction of the Crab nebula, together with a fit of a gaussian resolution curve of width 0.1° and a flat background.

Table 0.4 summarizes the performance of various HEGRA IACT observations of the Crab Nebula; as a measure serves the significance achieved in 1 h of observations, and the rate of events. The significance scales with $\sqrt{t}$ for not too short times, once background events appear under the signal. One hour of system observations is therefore equivalent to ≈7 hours of single-telescope observations, as far as the significance of the signal of a weak source is concerned. With improved analysis techniques, and the inclusion of the final system telescope CT2 - which increases the effective area of the system significantly - one expects to reach a performance of 8 to 10 sigma in one hour, for Crab observations. Improvements in the analysis concern the proper treatment of measurement errors - so far, all images are combined with equal weight, irrespective of the quality of an image - and the cuts to select γ-ray candidates; in the analysis shown here, only loose cuts were used, since the non-trivial optimization of multi-dimensional shape cuts has not yet been sufficiently studied.

Telescope	CT1	CT2	CT3	CT3-6
Mirror area[m^2]	5	8.5	8.5	4x8.5
Camera pixels	127	61	271	4x271
Pixel size[°]	0.25	0.43	0.25	0.25
field of view[°]	3.2	3.6	4.3	4.3
Energy threshold[TeV]	≈1.5	≈1.0	≈0.8	≈0.5
Trigger rate [Hz]	1	3	5	12
Crab detection rate[h^{-1}]	8	15	28	≈60
Crab-signal in 1 h	1.5	1.25	2.3	≈6

Tab. 0.4: Properties of the individual telescopes of HEGRA, and of the HEGRA CT system, as well as the performance for Crab observations.

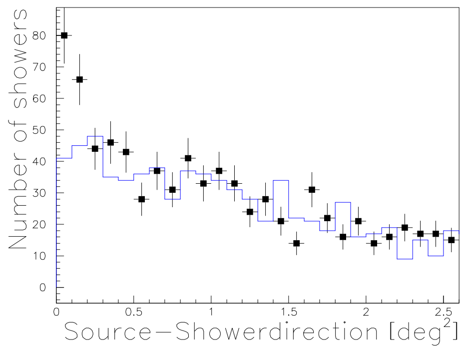

Fig. 0.17: Distribution of shower axes relative to the direction of the Crab Nebula of the 2 hour ON-OFF data set; the shower direction is reconstructed on the basis of the measured light arrival timing.

Since the IACT cameras allow to measure the arrival time of the light with a precision of about 1 ns, one can also use the timing to reconstruct the shower direction. Since the Cherenkov wavefront is slightly curved, it is however important to know the location of the shower core, in order to best fit the expected shape to the timing measurements. The core location is derived from the geometrical reconstruction based on image data. Fig. 0.17 illustrates that the showers can be reconstructed sufficiently well based on timing, to show a clear Crab signal.

The timing therefore provides an important cross-check for the shower reconstruction based on image shapes; ultimately, the two techniques will be combined for best resolution and background rejection.

[1] Mirzoyan R. et. al. , NIM A351, 513, 1994.
[2] Annual report MPIK Heidelberg p. 75, 1994.
[3] Annual report MPIK Heidelberg p. 101, 1995. Hermann G., "Entwicklung einer hochauflösenden Kamera für Abbildende Tscherenkov-Teleskope und Nachweis von TeV Gamma Strahlung aus der Richtung des Krebsnebels", PhD Thesis , 1996.
[4] A. Konopelko et al., Astroparticle Physics 4 (1996) 199.
[5] T.C.Weekes, Space Sci. Rev. 59 (1992) 315.
[6] D.Petry et al., Astron. Astrophys. 311 (1996) L13.
[7] M.Punch et al., Nature 358 (1992) 477.
[8] von Montigny C. et al., Ap.J. 440 (1996) 525.
[9] Li T.P. and Ma Y.Q.,Ap.J. 272 (1983) 317.
[10] J.Quinn et al., Ap.J. 456 (1996) L83.
[11] S.Bradbury et al., Astron. Astrophys., submitted.
[12] I.F.Mirabel and L.F.Rodriguez, Nature 371 (1994) 46.
[13] XVth European Cosmic Ray Symposium Pepignan (26. - 30. August 1996).
[14] G. Hermann, "Entwicklung einer hochauflösenden Kamera für Abbildende Tscherenkov Teleskope und Nachweis von TeV Gamma Strahlung aus der Richtung des Krebsnebels", PhD Thesis,Heidelberg 1996.
[15] M. Ulrich, "Eine neue Bildanalysemethode für Abbildende Atmospärische Cherenkov Teleskope und die zweidimensionale Richtungsrekonstruktion von TeV Photonen des Krebs-Nebels", PhD Thesis, Heidelberg 1996.
[16] G. Pühlhofer, "Aufbau der Steuerung für das Cerenkov Teleskop 3 des HEGRA Teleskop Systems", Heidelberg 1996, Diploma Thesis.
[17] A. Fraß, "Eine Methode zur Kalibrierung eines abbildenden Tscherenkow Teleskops", Diploma Thesis, will be ready in early 1997.
[18] H. Lampeitl, "Triggerung des HEGRA Cerenkov Teleskop Systems", Diploma Thesis, will be ready in early 1997.
[19] M. Heß, "Signalauslese von Cerenkov-Teleskopen mit Transientenrekordern", Heidelberg 1995, Diploma Thesis.

0.1.4 Source Models of VHE Gamma Radiation

Cosmic Rays and Gamma Rays in Supernova Remnants

E. Berezhko[a] , H.J. Völk

[a]Institute of Cosmophysical Research and Aeronomy, Lenin Ave. 31, 677891 Yakutsk, Russia

The kinetic models of cosmic ray nucleon acceleration in Supernova remnants (SNRs) that explode into a uniform interstellar medium have been completed. The emphasis is on the gamma-ray emission from such objects due to neutral pion decay. These fully nonlinear numerical models imply that CRs are accelerated with high efficiency (up to 50 percent at maximum). The main flux of high energy gamma-rays is produced during the early Sedov phase and decreases thereafter. The peak fluxes are by factors up to 7 higher than estimated previously.

We have completed our detailed kinetic model calculations of the cosmic ray (CR) nucleon acceleration and their gamma-ray production in SNRs which expand into a uniform interstellar medium [1]. The treatment is fully nonlinear and numerical. It is shown that the CRs are accelerated with very high efficiency: about 50% of the hydrodynamic explosion energy is converted into CRs at maximum during the SNR evolution, even for relatively low injection rates. The maximum energy reached by CR protons is about 10^{14}eV for a Bohm-limit diffusion coefficient. The main flux of high energy CRs is produced during the early Sedov phase and decreases thereafter. The results are compared with earlier models, based on the hydrodynamic approximation for CR transport and test particle estimates [2]. For a moderate ambient gas density of $0.3\ \mathrm{H-atoms\ cm^{-3}}$, corresponding to a warm interstellar medium, a magnetic field strength of 5μGauss, an explosion energy of 10^{51}ergs, the integral TeV gamma-ray flux from a SNR at a distance of 1kpc exceeds 10^{11}photons $\mathrm{cm^{-2}\ s^{-1}}$ at peak luminosity. This is higher than previously estimated peak fluxes by factors of the order of 7, and is primarily due to the combination of a harder spectrum, increased CR energy, and higher compression ratio. Spatially, SNRs without a central compact object are shell sources also in gamma rays throughout all their evolutionary phases. Given that such SNRs exist nearby they should be observable, in particular with sensitive ground based instruments.

[1] Berezhko, E., Völk, H.J. 1996, Astroparticle Phys., submitted

[2] Drury, L.O'C., Aharonian, F.A., Völk, H.J. 1994, A&A 287, 959

Synchrotron and inverse Compton nebulae around the pulsar PSR 1706-44

F.A.Aharonian, A.M.Atoyan[a], T.Kifune[b]

[a]on leave from Yerevan Physics Institute, Armenia

[b]Institute for Cosmic Ray Research, University of Tokyo

We interpret the TeV gamma radiation recently observed by the CANGAROO collaboration from the direction of the pulsar PSR 1706-44 as a result of inverse Compton scattering on the 2.7 microwave background radiation by electrons responsible also for extended X-ray nebula observed by ROSAT

Recently the CANGAROO collaboration has reported the positive detection of TeV gamma-ray radiation with a photon flux $I(\geq 1\,\mathrm{TeV}) \simeq 8\times10^{-12}\,\mathrm{cm^{-2}s^{-1}}$ from the direction of the pulsar PSR 1706-44. Although the possibility that this radiation represents the unpulsed component of the pulsar itself cannot be excluded, a more plausible interpretation of this radiation seems to be the inverse Compton (IC) scattering of ultra-relativistic electrons on 2.7 microwave background radiation (MBR). The same electrons would produce nonthermal X-ray nebula due to the synchrotron radiation in the ambient magnetic fields. Recently the observations by ROSAT revealed an extended X-ray nebula with angular size $\sim$ 0.5 arcmin surrounding the pulsar PSR 1706-44. The soft X-ray emission in the energy range 0.1-2.4 keV is fitted by a power-law spectrum which implies the existence of multi-TeV electrons in the nebula, and thus supports the hypothesis of the IC origin of the observed TeV radiation.

If the IC γ-ray and synchrotron X-ray components are produced in the same region, the ratio of the relevant energy fluxes above energies E and $\epsilon \simeq 0.07(E/1\,\mathrm{TeV})(\mathrm{B}/10^{-5}\,\mathrm{G})\,\mathrm{keV}$, depends only on the mean magnetic field B in that region: $f_\gamma(\geq E)/f_\mathrm{x}(\geq \epsilon) \simeq 0.1(B/10^{-5}\,\mathrm{G})^{-2}$. Since $f_\mathrm{x}(> 0.1\,\mathrm{keV}) \sim 3.2\times10^{-12}\,\mathrm{erg/s}$ observed by ROSAT (corrected for absorption) is almost an order of magnitude less than the observed flux of TeV γ-rays, the interpretation of the latter as of IC γ-rays would require, within a 'standard' approach, either extremely low magnetic field $B \leq 10^{-6}\,\mathrm{G}$ in the X-ray nebula around PSR 1706-44 (i.e. $3-5$ times less than in the conventional regions of the interstellar medium) or the existence of a dust far infrared radiation field with energy density as high as $w_\mathrm{FIR} \sim 5\,\mathrm{eV/cm^3}$ which could serve as a target photon field more efficient than the 2.7 K MBR. Such extreme assumptions on the ambient medium in the X-ray nebula could be significantly softened, if the observed X-rays are due to synchrotron radiation of electrons in the highest energy tail of the acceleration spectrum. For example, we show that marginal agreement between the observed and calculated X-ray/TeV γ-ray fluxes can be reached, assuming injection of relativistic electrons with an exponential cutoff at $E_\mathrm{e} \sim 20\,\mathrm{TeV}$, and $B \sim (3-5)\times10^{-6}\,\mathrm{G}$ in the X-ray nebula.

A more realistic scenario, however, seems the one assuming different spatial scales of the regions responsible for production of the X-ray and γ-ray fluxes detected. We show that these fluxes can be readily interpreted in terms of synchrotron X-ray and IC γ-ray radiations, if multi-TeV electrons injected into the compact X-ray nebula with an angular size of ≤ 0.5 arcmin and a magnetic field of $B \sim (1-3)\times10^{-5}\,\mathrm{G}$, would escape during several years into the surrounding interstellar medium with $B \leq 5\times10^{-6}\,\mathrm{G}$, forming a 'halo' of TeV γ-rays with angular size $\leq 0.1°$.

Constraints on the VHE Emissivity of the Universe from the Diffuse GeV Gamma-Ray Background

P.S. Coppi [a], F.A. Aharonian

[a]Yale University, USA

We re-examine and quantify the constraints placed on a cosmological VHE source population requiring that the secondary cascade radiation induced by primary photons with energy $\geq 100\,\mathrm{GeV}$ *in the diffuse extragalactic photon fields during the history of evolution* *of the Universe would not exceed the isotropic γ-ray background at GeV energies observed today.*

VHE (Very High Energy, $E \geq 100$ GeV) radiation emitted at cosmological distances pair produces on low-energy diffuse extragalactic background radiation before ever reaching us. This prevents us from directly seeing most of the VHE emission in the Universe. However, a VHE γ-ray that pair produces initiates an electromagnetic pair cascade. At low energies, this secondary cascade radiation has a spectrum insensitive to the spectrum of the primary $\gamma-$radiation and, unlike the original VHE radiation, *is observable.* Motivated by new measurements of the extragalactic MeV-GeV diffuse γ-ray background by the EGRET instrument aboard Compton GRO, we discuss the constraints placed on cosmological VHE source populations by requiring that the cascade background they produce does not exceed the observed levels. We use a new, accurate cascading code and pay particular attention to the dependence of the constraints on the diffuse cosmic background radiation. We have calculated the evolution of the diffuse extragalactic photon fields at infrared to ultraviolet wavelengths in different cosmological scenarios, and show that despite considerable uncertainty in this background, robust constraints may still be placed on the integrated emissivity of potential VHE sources in the Universe. Since the cascade photon flux falls in the 'GeV' energy region recently measured by EGRET, we can obtain a figure of merit for the maximum VHE emissivity of the Universe: $L_{\rm VHE} \leq 2 \times 10^{39}\,{\rm erg\,Mpc^{-3}s^{-1}}$. The limits are very tight, and restrict significantly, for example, the parameter space available for the exotic (e.g. *topological defect*) particle physics scenarios recently proposed to explain the highest energy cosmic ray events observed at energies above 10^{20} eV. Also, we show that if direct emission from blazar AGNs in fact accounts for most of the observed GeV background, these limits strengthen and rule out AGN emission models allowing for significant power above 100 GeV.

High energy emission from supernova remnant W44

O. de Jager[a], A. Mastichiadis

[a]Potchefstroom University, South Africa

The radio to gamma ray spectrum of the supernova remnant W44 has been fitted taking a detailed profile of the ambient matter and radiation known to exist by observations at other wavelengths. We deduce that the most plausible origin of the high energy radiation is a combination of relativistic bremsstrahlung/inverse Compton scattering by a population of very energetic electrons. The source of the radiating electrons is, most probably, a pulsar associated with the supernova remnant.

The EGRET experiment on board the Compton Gamma Ray Observatory has recently detected GeV emission from sources which can, with high confidence, be associated with supernova remnants (SNRs) [1]. Since SNRs have long been thought to be the sites of cosmic ray acceleration up to energies close to the knee [2], an analysis of the aforementioned observations could reveal interesting clues for the nature of the radiating particles and thus provide useful tests for existing theories for particle acceleration in SNRs.

The EGRET source 2EG J1857+0118 is located at the eastern border of the composite SNR W44 where the expanding radio shell is interacting with a dense molecular cloud. Using the inferred particle number density of the cloud, as deduced by CO observations, we have shown [3] that relativistic bremsstrahlung of the radio producing electrons can account for the bulk of the observed gamma ray emission. An extra component might be provided by the inverse Compton scattering of the same electrons on the infrared photons emitted by dust grains in W44.

Furthermore we find that the inferred energy content and spectral index of the radio/gamma-ray emitting electrons do not agree with the theoretical predictions of first order Fermi acceleration. Instead the injection of relativistic electrons by the pulsar PSR B1853+01 associated with the remnant seems to be a more viable hypothesis. In that case the injected energy would be sufficient to account for the required budget of the source if the initial spindown power of PSR B1853+01 is about 10 times larger than the present spindown power of the Crab pulsar.

Interestingly enough, a steeper Fermi electron component may be present but the observational data are not constraining enough to provide a meaningful limit on that possibility. At any rate, the predicted gamma-ray contribution from high energy proton-gas interactions is about 20% of the observed EGRET flux, which confirms the conclusion that the gamma-ray emission from W44 is dominated by a leptonic component.

[1] Esposito J.A. et al, 1996, Astrophysical Journal 461, 820.

[2] Lagage P.O., Cesarsky C.J., 1983 Astronomy & Astrophysics 125, 249.

[3] De Jager O., Mastichiadis A., 1997, Astrophysical Journal, in press.

0.1.5 Future CT System

F. Aharonian, W. Hofmann, A. Konopelko[a], M.Panter, H.J. Völk

[a]Altai State University, Barnaul, Russia

Comprehensive Monte Carlo studies and the analysis of the first stereoscopic observations of the Crab nebula with the HEGRA IACTs have demonstrated that the stereoscopic concept for IACTs works. In fact the results imply that the background signals from charged cosmic rays can be reduced to the size of the gamma-ray signal, i.e. that "background-free" ground based gamma-ray observations are possible. At the same time the hardware for the system of 5 IACTs of HEGRA has been essentially installed on La Palma. "Routine" observations will be possible, starting in the second half of 1997. Also the data acquisition system is in place and we will have to learn how to use it on a regular basis. The second and in the future dominant task will be to observe gamma-ray sources, in particular spatially extended sources, to determine their shape and energy spectrum, thereby learning to do astronomy with such a stereoscopic system.

While the HEGRA CT system has the highest priority for our institute, it is important to consider the future development of the field of ground based gamma-ray astronomy.

Given mainly by the mirror area of a single constituent IACT, the threshold of the HEGRA system is about 0.5 TeV. The sensitivity of the system is to lowest order given by the area coverage of the system, but it depends also on the threshold energy if the gamma-ray source spectra are sufficiently steep. Both factors together make the HEGRA CT system a medium sensitive instrument, just reaching in this regard the 10 m diameter single Whipple telescope in the US; HEGRA's qualities lie as much in its pioneering work on the aspect of stereoscopy as in its astronomical capabilities. In order to enhance these astronomical capabilities with a system of IACTs, the next generation IACT system beyond HEGRA should have somewhat lower threshold and higher sensitivity. A threshold of 100 GeV will on the one hand not imply new developments in the Cherenkov technique; especially the camera design developped in Heidelberg can be simply taken over. On the other hand, the absorption of Very High Energy gamma quanta in low energy Infrared/Optical photon fields limits the distance to which a gamma telescope can look. This then also limits the range of extragalactic astrophysics. A lower energy threshold of 100 GeV would increase the distance up to which extragalactic objects can be observed without absorption to a redshift of z $\sim$ 1 which opens the way to attack many questions of physical cosmology, like the epoch of galaxy formation, or the absolute distance scale (i.e. the Hubble constant) at such redshifts. In general this lower threshold will also increase the sensitivity of the instrument. At the same time the threshold is still high enough to pursue the essential goals of TeV gamma-astronomy. At given threshold the sensitivity can only be increased by covering larger regions on the ground with IACTs. The reason is that the effective area of an IACT is -at given threshold energy- given by the characteristics of the atmosphere which acts as the target for the shower and the Cherenkov light development. Independently of HEGRA we are therefore planning a future large system of IACTs with somewhat larger telescope mirrors ($\sim$ 12m diameter) allowing an energy threshold of 100 GeV. An initial array would consist of a system of 4 telescopes (IACTs) on a square of size $\sim$ 100m, to be extended subsequently to a 3 by 3 and 4 by 4 array. The required plane surface area of such an observatory would be about 350 m by 350 m at a height of about 2000 m above sea level. Contacts with industry show that the telescope frames could be readily built. The focal plane instrumentation would use simmilar technologies as the existing HEGRA cameras. A most important factor is the infrastructure at a site with the optical quality of an astronomical observatory in the optical wavelength range. The investigation of possible sites has been discussed extensively, in particular with our colleagues at the MPI für Astronomie who run the Spanish-German observatory of Calar Alto in southern Spain. A Letter of Intent is in preparation.